Enzyme-free Immunoassay for Rapid, Sensitive, and Selective Detection of C-reactive Protein

Sathishkumar Munusamy, Haiyan Zheng, Rana Jahani, Shuo Zhou, Jun Chen, Juanhua Kong and Xiyun Guan*

Author affiliation:

Department of Chemistry, University of Missouri, Columbia, MO 65211, USA

*Corresponding Author E-mail: xgpc2@missouri.edu

Abstract

C-reactive protein (CRP) is a protein made by the liver, which is released into the bloodstream in response to inflammation. Furthermore, CRP is a potential risk factor for heart disease. Hence, it is of great importance to develop a rapid, sensitive, accurate and cost-effective method for CRP detection. Herein, we report an enzyme-free fluorescent assay for the rapid and ultra-sensitive detection of CRP with a limit of detection (LOD) reaching as low as 3.08 pg/mL (i.e., ~ 27 fM). The high sensitivity of our method was simply achieved via dual-functionalized gold nanoparticles (AuNPs). By regulating the molar ratio of DNA to CRP antibody immobilized on the AuNP surface, hundreds to thousands-fold amplification in the analyte signal could be instantly accomplished. Furthermore, our sensor was selective: non-target proteins such as interleukin-6, interleukin-1β, procalcitonin, bovine serum albumin, and human serum albumin did not interfere with the target CRP detection. Moreover, simulated serum samples were successfully analyzed. Given the excellent sensitivity, selectivity, and high resistance to complicated matrices, the enzyme-free CRP detection strategy developed in this work can be used as a generic platform to construct sensors for a wide variety of protein biomarkers and hence offers the potential as a tool for rapid, accurate, and low-cost medical diagnosis.

Keywords: Enzyme-free Immunoassay, AuNPs, Fluorescent assay, CRP protein, Amplification

Introduction

With the development of biomedical technology and data science, more and more biomarkers such as nucleic acids, proteins, enzymes, and metabolites are being discovered[1–4]. Given the important roles these biomolecules play in a wide variety of biological and pathological processes and drug discovery, analysis of biomarkers in biofluids is of great significance for disease prevention, early diagnosis, and prognosis[5–8]. Therefore, there is a need for advanced biosensing techniques for rapid, affordable, highly sensitive, and accurate detection of biomarkers in complicated matrices. Thus far, various protein detection methods have been developed, including conventional such as enzyme-linked immunosorbent assay (ELISA) and more recent nano-biosensing techniques. Briefly, as one of the most popular methods for protein detection, ELISA has the advantages of good selectivity and high resistance to matrix effect and is considered as the gold standard for routine protein analysis in clinical samples[9–13]. However, the application of ELISA is limited by time-consuming and labor-intensive procedures as well as the unsatisfactory sensitivity toward many protein biomarkers at ultra-low concentrations in clinical samples. In contrast, lateral flow immunoassays (LFAs) provide a point-of-care testing (POCT) diagnostic platform for rapid, user-friendly, and cost-effective protein detection [14–18]. However, the conventional LFA test suffers from poor sensitivity, leading to large false positive or false negative rates. To improve the sensitivity of protein assay, numerous nano-biotechnologies (biosensors) based on fluorescence, colorimetric, electrochemical, and resonance measurement, as well as nanopore sensing, have been developed recently[19–28]. Although these biosensors have reported significantly lower LODs than ELISA, the majority of them rely on time-consuming enzymatic reactions or other chemical reactions, such as click reactions, hybridization chain reactions, etc., to amplify signals. The requirement for specific reaction conditions and the need for an extra sample incubation procedure to achieve signal amplification make these new nano-biosensing methods at a disadvantage in rapid protein detection.

Herein, we report an enzyme-free fluorescent assay for the rapid and ultra-sensitive detection of proteins in complicated matrices. The high sensitivity of our method was achieved via dual-functionalized gold nanoparticles (AuNPs). Due to their substantial specific surface area, excellent biocompatibility, straightforward preparation process, and robust stability, AuNPs are widely utilized as nanocarriers to explore various applications[29–34]. By regulating the molar ratio of

barcode DNA to target protein antibody immobilized on the AuNP surface, hundreds to thousands-fold amplification in the analyte signal could be instantly accomplished. In this work, C-reactive protein (CRP) is used as a model protein to demonstrate the feasibility of this rapid and sensitive protein assay[35–42]. CRP is one of the most important clinical markers for chronic inflammation. Produced by the liver under the influence of interleukin-6, interleukin-1β, and tumor necrosis factor, elevated CRP levels indicate inflammation, aiding in diagnosing and monitoring inflammatory conditions and related diseases[43–48]. Furthermore, CRP is a potential risk factor for heart disease[49, 50]. Similar to other proteins, various methods have been developed for CRP detection, including ELISA, LFA, surface-enhanced Raman, colorimetric, luminescence, SPR, and electrochemical methods, with LODs ranging from 66 pg/mL to 286 ng/mL[36, 38, 40, 51–55].

Experimental section

Materials and Reagents

The human serum albumin (HSA), bovine serum albumin (BSA), interleukin-6 (IL-6), interleukin-1β (IL-1β), procalcitonin (PCT), Tween-20 and human serum (from human male AB plasma, USA origin) were purchased from Sigma-Aldrich (St. Louis, MO). CRP protein and paired (capture and detection) monoclonal anti-CRP antibodies were purchased from Medix Biochemica (St. Louis, MO). Single strand DNAs P1 (a 20-mer poly(dT) connected with a C6 spacer and a terminal disulfide bond at 5' end; sequence: HS-S-$(CH_2)_6$-TTTTTTTTTTTTTTTTTTTT) and P2 (a 20-mer poly(dA); sequence: AAAAAAAAAAAAAAAAAAAA) were obtained from Integrated DNA Technologies (Coraville, IA). Magnetic beads (Dynabeads™ M-270 Carboxylic Acid) of 2.8 μm diameter were obtained from Invitrogen (Carlsbad, CA). Gold colloids solutions of various sizes (15, 30, and 50 nm diameter) were purchased from Nanopartz (Loveland, CO). Single-strand DNA specific binding dye (QuantiFluor® ssDNA System) was purchased from Promega Corporation (Madison, WI). All the reagents were used directly without further treatment unless otherwise stated. The assay buffer (pH 7.2) consists of 0.1 M NaCl, 0.025% Tween-20, 0.1% BSA, and 10 mM PBS.

Preparation of functionalized magnetic beads (MBs)

The procedure for preparing the CRP capture antibody-functionalized magnetic beads is shown in Scheme S1. Briefly, 200 μL (~2 x 10^9 beads/mL) of magnetic beads (MBs) were washed three times with 200 μL of MES buffer (25 mM, pH 5.0). After washing, the beads were resuspended in 200 μL of MES buffer (25 mM, pH 5.0). Then, 100 μL of N-(3-Dimethylaminopropyl)-N'-ethylcarbodimide hydrochloride (EDC) (50 mg/mL) and 100 μL of N-Hydroxysuccinimide (NHS) (50 mg/mL) were added to the suspension. After a 30-minute incubation at room temperature with agitation, the MBs were separated from the supernatant and underwent three additional washes with MES buffer. Then, 100 μL of CRP capture antibody (Ab_1, 1 mg/mL) was added to the obtained carboxyl-activated MBs in 100 μL of MES buffer and incubated for 30 minutes at room temperature with rotational agitation. Subsequently, the antibody-functionalized MBs underwent three washes with 100 μL of phosphate-buffered saline (PBS, pH 7.4), followed by being blocked with 50 μL of 0.05% (w/v) BSA for 10 minutes (with vortexing), and were finally resuspended in 500 μL of PBS for subsequent applications. The successful synthesis of CRP capture antibody-conjugated MBs (MBs-Ab_1) was verified by determining the amount of antibodies bound to the MBs, which was obtained by measuring the change in the UV-vis absorbance of the CRP capture antibody solution at 280 nm before and after MBs conjugation (Fig. S1). The coupling efficiency of the MBs with the monoclonal CRP antibody was found to be 68.8%.

Preparation of dual functionalized AuNPs

The procedure for preparing dual functionalized AuNPs are shown in Scheme S2. Briefly, CRP detection antibody (Ab_2) was first immobilized to AuNPs via the spontaneous adsorption by incubating a solution mixture containing colloidal AuNPs (ranging from 11.72 to 459 μL and from 7.41 to 290 nM), 5 μL of 2 M NaOH, and 2.5 μL of CRP detection antibody (Ab_2, 100 μg/mL) at room temperature for 30 minutes. The resulting Ab_2-AuNP conjugate was resuspended in 100 μL of 0.02% Tween-20. Then, as described in our published work[56], disulfide-terminated DNA was reduced by treating it with tris(2-carboxyethyl)phosphine (TCEP) for 1 hour at room temperature to yield thiol-terminated DNA (P1, 100 μL, 100 μM), which was then mixed with the obtained CRP detection antibody-functionalized AuNPs (Ab_2-AuNPs) and an additional 800 μL of 0.02% Tween 20, allowing for reaction at ambient temperature for 1 h. After that, to facilitate the uptake of AuNPs, the "aging-salting" process was executed. Briefly, the functionalized Ab_2-AuNP-P1

mixture was added with 2 M NaCl to gradually increase the concentration of NaCl to 0.3 M and incubated overnight[57]. Then, the solution was centrifuged at 10,000 × g for 10 min to separate the Ab_2-AuNP-P1 from the unreacted reagents. The product (Ab_2-AuNP-P1) was then converted to Ab_2-AuNP-P1-P2 by adding 10 µL of 1 mM complimentary ss-DNA P2. After purification through three cycles of centrifugation, the final product was resuspended in ultra-pure HPLC-grade water, and stored at 4°C. Although we could not quantify the number of antibodies immobilized on AuNPs due to the very low concentration, we were able to determine the number of DNA attached to AuNPs by measuring the change in the UV-vis absorbance of the DNA solution at 260 nm before and after AuNPs conjugation (Fig. S2). The loading efficiency obtained was ~1,100 DNA molecules per AuNP of 30 nm diameter, which was estimated based on the following equation.

$$DNA\ loading\ density = \frac{Concentration\ of\ DNA\ attached\ on\ AuNPs}{Final\ concentration\ of\ AuNPs}$$

Characterization of Ab_2-coated AuNPs

Transmission electron microscopy (TEM) images were acquired using a JEOL JEM-1400 instrument operating at an accelerating voltage of 120 kV. Samples were prepared by drop-casting onto carbon-coated copper grids and left to dry for 24 hours prior to analysis. Particle size distribution was determined using ImageJ software. Dynamic light scattering (DLS) analyses were performed using a Zetasizer Nano ZS (Malvern Panalytical). The viscosity of the sample was presumed to match that of the dispersant, water, with a value of 0.8872 cP and a refractive index (RI) of 1.330. The measurements were conducted at a controlled temperature of 25 °C, following a 10-second equilibration period. Each sample underwent triplicate analysis, with the measurement duration set to automatic. The measurements were taken at a 173° backscatter angle, with automatic adjustment of both the positioning and attenuation.

Procedure for CRP assay

To detect CRP, CRP capture antibody-functionalized MBs were resuspended in 1 mL of assay buffer after three times washing of 50 µL of the prepared Ab_1-MBs with 500 µL assay buffer. Then, CRP standard solution with the concentration ranging from 10 pg/mL to 1 ng/mL was added, and

the mixture was incubated for 1 hour using a rotary mixer at room temperature. After that, a magnet field was applied to remove the supernatant, followed by three times washing and resuspended in 500 µL assay buffer. Then, the dual functionalized AuNPs (Ab_2-AuNP-P1-P2) were added to the MB-Ab_1-CRP complex solution, and incubated for 1 h at ambient temperature to form the sandwich structure (i.e., MB-Ab_1-CRP-Ab_2-AuNP-P1-P2). After separating the sandwich complex with the supernatant and additional three times washing with assay buffer, 100 µL of HPLC water was added, followed by heating at 70°C for 15 minutes to release ssDNA P2 from the sandwich complex. The mixture was then separated, and the supernatant was collected. The obtained P2 solution was used for fluorescence measurement after adding 100 µL of ssDNA selective dye, which was obtained after diluting the QuantiFluor® ssDNA Dye by 2,000x in 1X TE buffer.

Results and discussion

Principle of the enzyme-free DNA barcode amplification immunoassay for CRP

Briefly, as shown in Figure 1, the procedure of our designed enzyme-free DNA barcode amplification protein detection consists of 5 major steps: 1) protein samples are incubated with capture antibody-conjugated magnetic beads (MB-Ab_1). After magnet separation, target proteins (TP) are captured on MB-Ab_1, leading to the formation of MB-Ab_1-TP, while the other components in the sample are discarded; 2) Dual-functionalized gold nanoparticles conjugated with detection antibody and dsDNA (Ab_2-AuNP-dsDNA or more specifically Ab_2-AuNP-P1-P2) are mixed with MB-Ab_1-TP to form sandwich structures (MB-Ab_1-TP-Ab_2-AuNP-P1-P2), thus introducing dsDNA (note that only one strand (i.e., P1 in our work) of the dsDNA is terminal thiolated so that it can bind to AuNPs tightly via Au-S bond, while the other strand (P2) can be released if necessary); 3) After the sandwich product is washed repeatedly and redispersed in HPLC-grade water, the DNA duplexes on AuNPs are de-hybridized (e.g., by heat denaturation) to release the reporter ssDNA (P2), which will then be separated from the sandwich complexes by using a magnetic field; and 4) a ssDNA specific binding dye will be added to the reporter ssDNA-containing solution, followed by fluorescence measurement. Note that in our designed enzyme-free protein detection strategy, the dual-functionalized AuNPs play a critical role in the sensor sensitivity. By controlling the molar ratio of dsDNA to detection antibody on the AuNP surface, hundreds to thousands-fold increase in the analyte signal could be instantly achieved without an

extra amplification reaction step as used in many of the other protein detection strategies. In this work, CRP is used as a model protein to demonstrate the feasibility of this rapid and sensitive protein detection method.

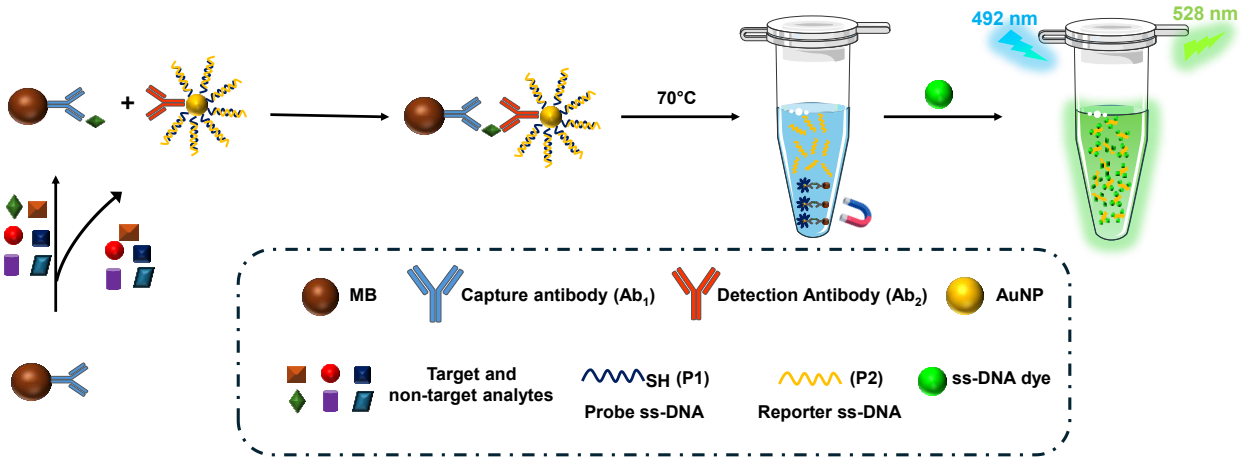

Figure 1. Schematic representation of the enzyme-free DNA barcode amplification immunoassay for rapid and sensitive detection of CRP (not to scale).

Effect of CRP detection antibody immobilized on the AuNPs surface on CRP detection

As mentioned previously, a distinguishing feature of this work from other protein detection studies lies in that a unique DNA barcode amplification (via AuNPs dual-functionalized with detection antibody and dsDNA) is designed to significantly boost the sensor sensitivity. By controlling the molar ratio of detection antibody to dsDNA on the AuNP surface, hundreds to thousands-fold increase in the analyte signal could be instantly achieved. Hence, in principle, a decrease in the number of antibodies on AuNPs would lead to an increase in the sensor sensitivity. Unfortunately, due to the small amount of antibodies immobilized, quantitative measurement of the antibody loading density on AuNPs is not viable. To highly sensitively detect CRP, CRP detection antibody functionalized AuNPs (Ab_2-AuNP) were prepared by incubating various concentrations of Ab_2 (2.5, 5 and 10 μg/mL) with AuNPs (30 nm in diameter, 0.004 μM). UV–vis absorption spectroscopy analysis was performed to confirm the successful decoration of Ab_2 on AuNPs, and the results were shown in Fig. S3. Clearly, before modification, the AuNP solution showed a strong surface plasmonic resonance (SPR) absorption peak at ~521 nm (black curve). In contrast, after

modification, an SPR peak (~525 nm) with a red shift of 4 nm was observed with reduced absorption intensity, suggesting the triumphant capping of Ab_2 on AuNP surfaces (red curve) (Fig. S3). TEM was employed to characterize the morphology and determine the size of the AuNPs before and after conjugation with the antibody Ab_2. We found that the bare AuNPs were predominantly spherical and uniformly distributed (Fig. 2A), with an average size of 28.9 ± 2.4 nm, and exhibited a narrow size distribution (Fig. 2B). In contrast, the TEM image of the Ab_2-conjugated AuNPs (Ab_2-AuNPs) showed a distinct shadow around the surface of the nanoparticles (Fig. 2C, highlighted in red arrows), which was absent in the unmodified AuNPs, indicating the presence of an organic coating. Moreover, after Ab_2 conjugation, the particle size increased by 2 nm (Fig. 2D). This coating was further confirmed by negative staining of the Ab_2-AuNP samples (Fig. 2E, highlighted in red arrow). DLS measurements indicated that the hydrodynamic diameter increased from 68 nm for the bare AuNPs to 75 nm after Ab_2 conjugation (Fig. 2F). As anticipated, the DLS-derived diameters were larger than those measured by TEM (28.9 nm vs. 68 nm), attributed to the double-layer effect considered in the hydrodynamic radius calculations for particles in solution, which is absent in the dried-state samples observed in TEM. Additionally, DLS measurements are influenced by factors such as viscosity and temperature[58].

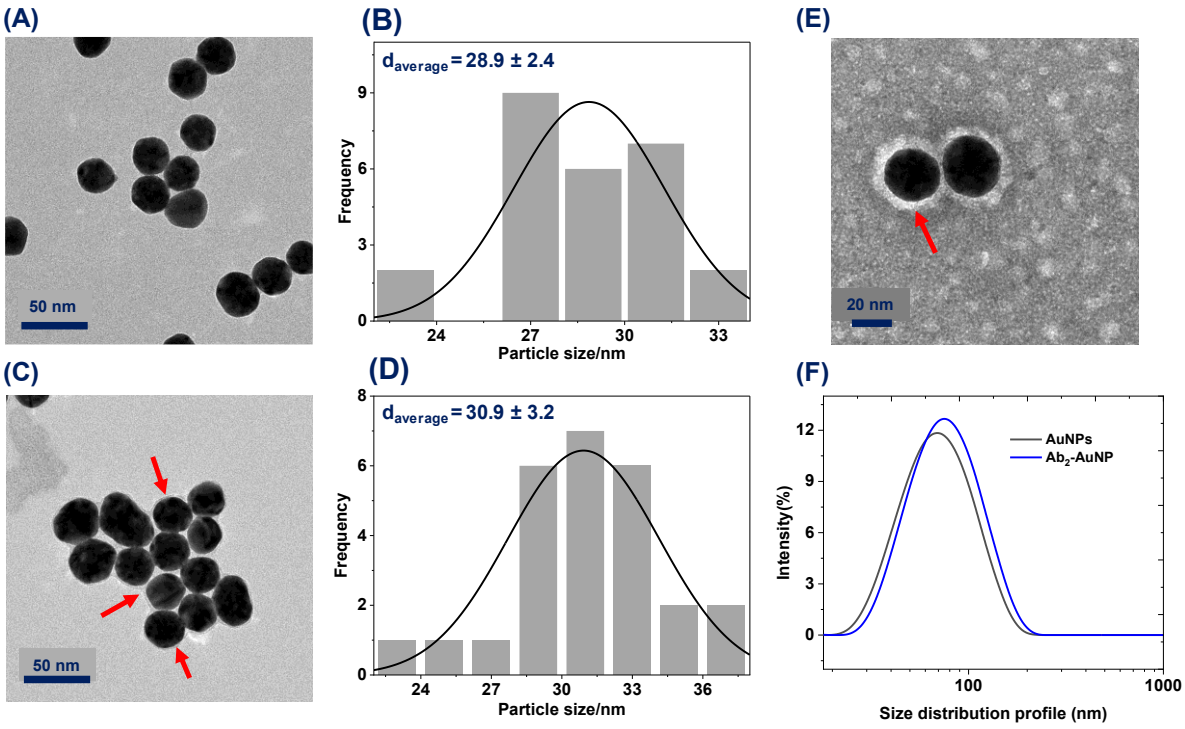

Figure 2. (A) TEM image of bare AuNPs, illustrating the size and shape of the synthesized nanoparticles. Scale bar: 50 nm; (B) Particle size distribution curve of bare AuNPs; (C) TEM image of Ab_2-conjugated AuNPs (Ab_2-AuNPs). Scale bar: 50 nm; (D) Particle size distribution curve of Ab_2-AuNPs; (E) TEM image of Ab_2-AuNPs after negative staining. Scale bar: 20 nm; and (F) Size distribution analysis of AuNPs and Ab_2-AuNP by dynamic light scattering. The experiment shown in Fig. 2E was carried out by applying a small drop (~ 5-10 μL) of 0.5% uranyl acetate solution to the TEM grid to cover the Ab_2-AuNPs sample. After incubation for 30 seconds to 1 minute for sufficient background staining, the grid was air-dried thoroughly at room temperature before imaging in the electron microscope. Uranyl acetate stains the background, making the sample appear as a negative (unstained) image.

After incubation with 10 μM of DNA P1, the as-prepared Ab_2-AuNP-P1 conjugates having various Ab_2 loading densities were then converted to Ab_2-AuNP-P1-P2 (by addition of the complementary ssDNA P2 strands), followed by forming a sandwich structure with MB-Ab_1 and the CRP protein. After dehybridization, P2 was collected and quantified by addition of ssDNA staining dyes, followed by fluorescence measurement. To ensure that the Ab_2 effect on sensor sensitivity is representative, two CRP concentrations (50 pg/mL and 500 pg/mL) were examined. The experimental results were summarized in Fig. 3A & B and Figs. S4 & S5. Clearly, in both cases, with an increase in the Ab_2 concentration (from 2.5 μg/mL to 10 μg/mL), a decrease in the fluorescence intensity (from 1280 to 290, and from 7890 to 1350, respectively) for the CRP samples was observed, while the fluorescence signal of blank did not change significantly. Therefore, a decrease in the Ab_2 concentration led to an increase in the signal-to-noise ratio and hence a higher sensor sensitivity. This experimental result supports our hypothesis that by increasing the molar ratio of DNA to Ab_2 on the AuNPs surface, an increase in the analyte signal could be instantly achieved.

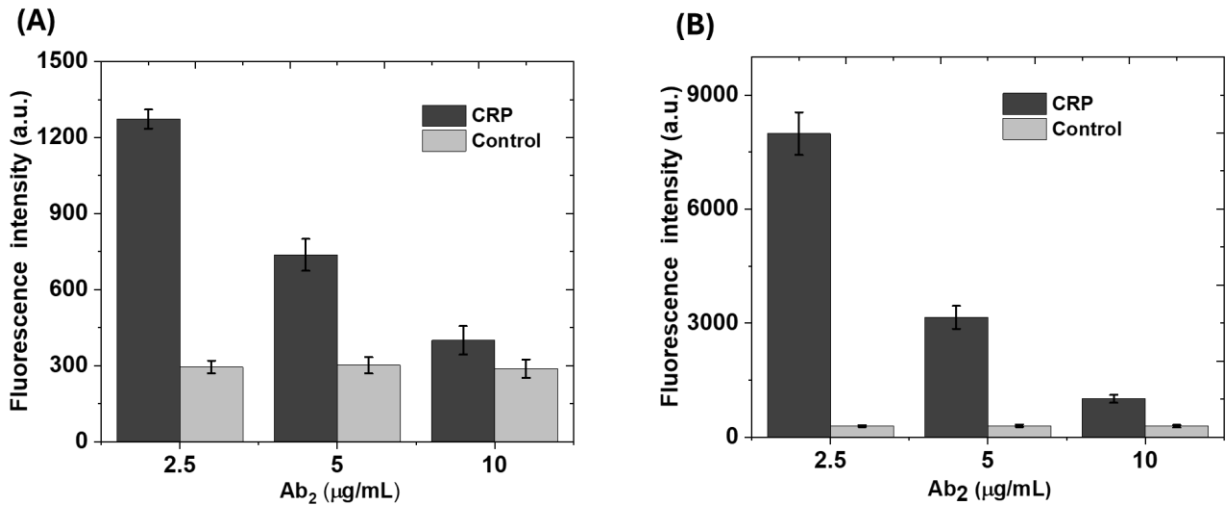

Figure 3. Effect of CRP capture antibody used for preparing dual functionalized AuNPs on the detection of (A) 50 pg/mL and (B) 500 pg/mL of CRP. Fluorescence measurement was performed with $\lambda_{ex/em}$ = 492/528 nm at room temperature. Each data point represents the average from three replicate analyses ± one standard deviation.

Effects of AuNP diameter on the sensor sensitivity

The dual-functionalized AuNPs play a critical role in the sensitivity and the selectivity of the enzyme-free CRP sensor. In particular, the surface area of AuNPs determines the total number of antibody and DNA molecules which can possibly be conjugated to AuNPs. In general, the larger AuNP diameter, the more antibody and DNA molecules can be immobilized, and hence a larger DNA to antibody ratio and a larger analyte signal amplification can be achieved. However, on the other hand, as the AuNP diameter increases, the size of the formed dsDNA-AuNP-Ab_2 complex will also increase. Compared with small-size dsDNA-AuNP-Ab_2 complexes, fewer large-size dsDNA-AuNP-Ab_2 complexes can be immobilized on the surface of MB-Ab_1 to form sandwich structures. Accordingly, if MBs are full of antibodies, each of which has captured a CRP molecule, large dsDNA-AuNP-Ab_2 complexes may not be able to bind to all of the target CRP molecules due to the steric effect, leading to a decrease in the sensor sensitivity. Furthermore, one challenge when working with large-diameter AuNPs is that they are prone to aggregation[59, 60], especially

when antibodies are attached to their surface. Therefore, to optimize the sensor sensitivity, the effect of spherical AuNP diameter on DNA loading and CRP detection needs to be investigated.

To explore the relationship between the size of AuNPs and DNA loading, three DNA-functionalized AuNPs with different diameters were examined. These DNA-AuNP conjugates (formed via Au-S bond) were constructed by immobilizing DNA P1 (100 μL, 0.1 mM) to the surface of AuNPs of 15 nm (11.72 μL, 290 nM), 30 nm (100 μL, 34 nM), and 50 nm (459 μL, 7.41 nM) in diameter, respectively using a rapid salt aging method combined with sonication [61]. We found that, as the diameter of the AuNPs increased from 15 to 50 nm, DNA uptake escalated from 310 to 1350 molecules per AuNP (Fig. 4A). Further study (Fig. 4B) showed that, although increase of P1 concentration to 15 μM could lead to an increase in the number of immobilized DNA per AuNP, the effect was not significant, indicating the saturation effect or altered binding kinetics at higher P1 concentrations.

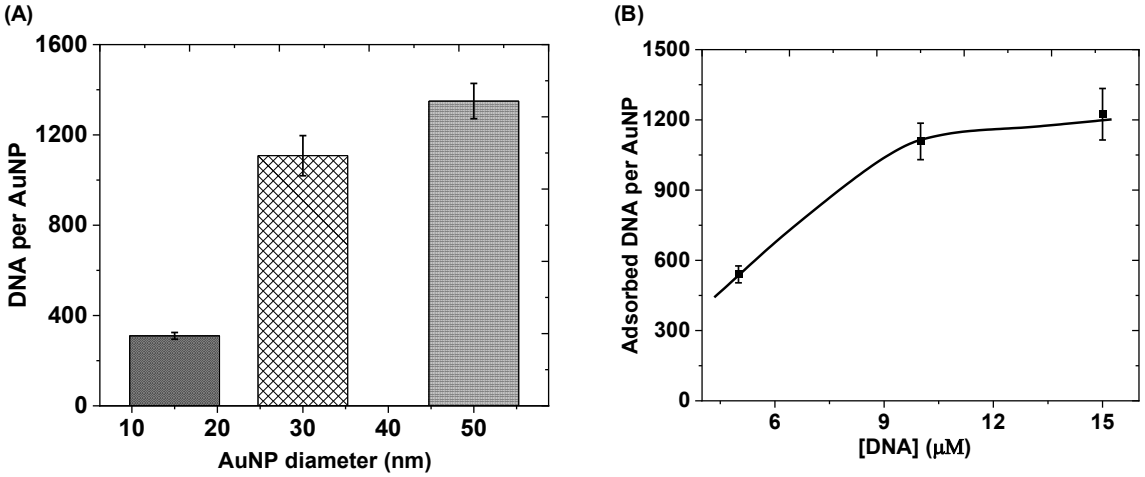

Fig 4. Effects of (A) AuNP diameter and (B) DNA concentration on DNA loading density on the surface of AuNPs. The experiments shown in Fig. 4B were performed in the presence of 100 μL of 34 nM of AuNPs of 30 nm in diameter.

To assess the effect of AuNP diameter on CRP detection, three CRP detection antibody and DNA dual-functionalized AuNPs (Ab_2-AuNP-P1-P2) with different diameters were examined. The Ab_2-AuNP-P1-P2 complexes were constructed using a two-step conjugation procedure as described in

the experimental section. Briefly, AuNPs of 15, 30, and 50 nm diameters were first incubated with Ab_2, followed by P1, and then hybridized with P2. The as prepared Ab_2-AuNP-P1-P2 conjugates were used together with MB-Ab_1 to detect 500 pg/mL of CRP according to our designed enzyme-free strategy. We found that, among the three dual-functionalized AuNPs, the one with 30 nm diameter showed the largest fluorescence intensity, while the 50 nm diameter AuNP yielded the smallest fluorescence signal (Fig. 5). The results are not unreasonable considering that the lesser DNA uptake is allowed on the surface of 15-nm AuNP than 30-nm AuNP, leading to a decrease in the analyte signal amplification. On the other hand, there are two likely reasons why the 50 nm diameter AuNP showed reduced sensor sensitivity. First, it is well known that AuNPs are prone to aggregation, especially when their sizes are large and in the presence of antibodies. Second, large Ab_2-AuNP-P1-P2 complexes may not be able to bind to all of the target CRP molecules captured by the Ab_1-MB conjugate due to the steric effect. Therefore, 30 nm diameter was deemed as the optimal AuNPs size, and used in the remaining experiments.

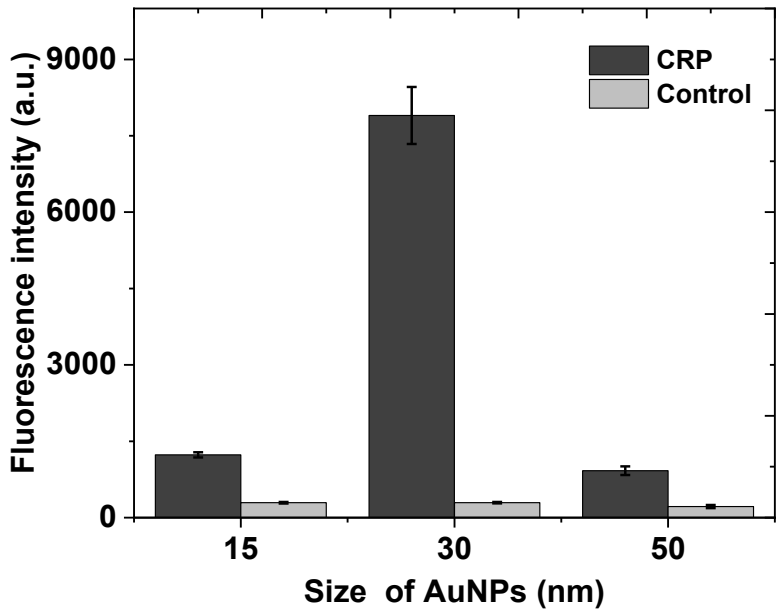

Figure 5. Effect of AuNP diameter on the sensitivity of the CRP sensor. Fluorescence measurement was performed with $\lambda_{ex/em} = 492/528$ nm at room temperature. Each data point represents the average from three replicate analyses ± one standard deviation.

Sensitivity and selectivity of CRP detection

Using the optimized dual-functionalized AuNPs (30 nm diameter AuNPs, 2.5 μg/mL of Ab_2, and 10 μM of P1), a series of CRP proteins with different concentrations ranging from 10 pg/mL to 1 ng/mL was examined using our constructed enzyme-free fluorescence sensor. We found that the fluorescence intensity of the solution increased linearly with an increase in the CRP concentration (Fig. 6A & 6B). The limit of detection (LOD, which is defined as the CRP concentration corresponding to three times the standard deviation of a blank signal) of the CRP sensor was as low as 3.08 pg/mL. As far as we are aware, such a LOD is as good as those (ranging from 0.01 pg/mL to 0.39 ng/mL) of various other sensitive CRP detection methods such as SERS[38, 62], SPR[53], colorimetric [54], electrochemiluminescence[36, 40, 63], chemiluminescence[64], and electrochemical measurement techniques [51, 55, 65]. Given that the CRP concentrations in the serum of healthy population were 10 - 100 μg/mL, our method is sensitive enough to analyze clinical samples for infection and inflammation[49, 66] diagnosis without sample pretreatment. Such a high sensor sensitivity is very impressive since, unlike ELISA and the majority of other detection techniques, our method did not involve measuring the activity of an enzyme or relying on complicated chemical reactions to amplify the signals, so that an extra time-consuming incubation step is not needed.

To determine the selectivity of this enzyme-free CRP sensor, a series of proteins were then analyzed, including IL-6, IL-1β, PCT, BSA and HSA. Similar to CRP, IL-6, IL-1β, and PCT are important inflammatory markers[67–72]. In contrast, BSA is the most abundant plasma protein in bovines and is often used as a protein concentration standard in lab experiments, while HSA is the most abundant blood protein in humans. As shown in Fig. 6C, a large fluorescence signal was observed in the presence of CRP, while addition of other proteins to the solution only resulted in similar fluorescence signals to that of the blank sample, and hence can be negligible. The results suggest that our sensor is highly selective to CRP due to the specific antigen–antibody binding.

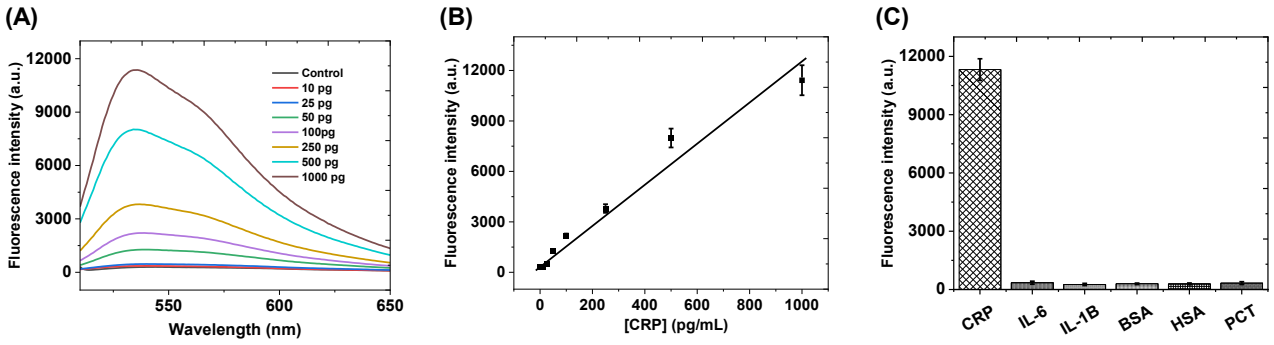

Figure 6. (A) Fluorescence spectra, showing the effect of CRP concentration on fluorescence intensity; B) dose-response curve for CRP; and C) sensor selectivity study. Fluorescence measurement was performed with $\lambda_{ex/em} = 492/528$ nm at room temperature. The concentrations of the proteins in Fig. 6c were 1000 pg/mL each.

Quantitative Analysis of CRP in Simulated Seum Samples

One of the significant advantages of sandwich assays is their ability to specifically detect the target analyte in complicated matrices such as bodily fluids. To demonstrate the viability of utilizing our developed CRP sensor for clinical sample analysis, four mock human serum samples were examined. These samples were prepared by spiking CRP standard solutions with final concentrations ranging from 50 to 500 pg/mL to human serum (Sigma-Aldrich). These samples were analyzed by our enzyme free sensor without further dilution. As shown in Table 1, the recoveries obtained by use of our developed fluorescence assay ranged from 102.4 to 124.2%, with the relative standard deviation less than 8.6%. The experimental results suggest that our developed CRP fluorescence sensor has high resistance to the serum matrix even when the CRP concentration is very low, and hence offers a potential use as a tool in clinical diagnosis.

Table 1. Recovery of CRP from simulated human serum samples

Sample Number	Theoretic Value (pg/mL)	Experimental Value[a] (pg/mL)	Recovery (%)
1	50	62.2 ± 3.2	124.2 ± 4.9
2	100	102.4 ± 2.2	102.4 ± 3.8
3	250	260.6 ± 7.6	104.2 ± 8.6
4	500	524.0 ± 5.3	104.8 ± 3.7

[a]Each experimental value represents the mean of three replicate analyses ± one standard deviation.

Conclusion

In summary, a pioneering enzyme-free fluorescent assay was developed for the rapid and sensitive detection of CRP with a LOD reaching as low as 3.08 pg/mL (i.e., ~ 27 fM). Unlike the majority of various protein detection techniques reported thus far, which rely on time-consuming enzymatic reactions or other chemical reactions such as click reaction, hybridization chain reaction, etc. to amplify signals, the high sensitivity of our method is simply achieved via dual-functionalized AuNPs. By regulating the molar ratio of DNA to antibody immobilized on the AuNP surface, hundreds to thousands fold increase in the analyte signal can be instantly accomplished. It should be noted that the sensor response to the CRP samples reported in this work were obtained based on the measurement of the fluorescence intensity of the collected ssDNA reporter solutions after addition of ssDNA specific binding dyes. The sensitivity and LOD of our pioneered DNA barcode amplification strategy for protein detection might be further improved by quantitating the collected reporter DNA using other readout formats. Given the excellent sensitivity, selectivity and high resistance to complicated matrices, the enzyme-free CRP detection strategy developed in this work may be used as a generic platform to construct sensors for a wide variety of protein biomarkers, and hence offers the potential as a tool for rapid, accurate, and low-cost medical diagnosis.

ASSOCIATE CONTENT

Supporting Information

The Supporting Information is available free of charge on the Publications website.

Additional schemes and figures, including fabrication of CRP capture antibody-functionalized MBs, preparation of dual-functionalized AuNPs with CRP detection antibody and dsDNA, UV-vis spectra of CRP solution before and after MBs conjugation, UV-vis spectra of DNA solution before and after AuNPs conjugation, and UV-Vis spectra of AuNPs before and after antibody conjugation.

AUTHOR INFORMATION

Corresponding author

E-mail: Xiyun Guan (xgpc2@missouri.edu).

CRediT authorship contribution statement

SathishKumar Munusamy: Conceptualization, Methodology, Investigation, Formal analysis, Data curation, Writing – original draft. **Haiyan Zheng:** Investigation. **Rana Jahani:** Investigation. **Shuo Zhou:** Investigation. **Jun Chen:** Investigation. **Juanhua Kong:** Investigation. **Xiyun Guan:** Conceptualization, Supervision, Project administration, Funding acquisition, Writing – review & editing.

Declaration of Competing Interest

The authors declare no competing financial interests.

ACKNOWLEDGMENT

This work was financially supported by the National Institutes of Health (R01GM147247) and National Science Foundation (2203763 and 2345813).

References

1. Chen F, Di T, Yang C-T, Zhang T, Thierry B, Zhou X (2020) Naked-Eye Enumeration of Single Chlamydia pneumoniae Based on Light Scattering of Gold Nanoparticle Probe. ACS Sens 5:1140–1148.

2. Tao G, Lai T, Xu X, Ma Y, Wu X, Pei X, Liu F, Li N (2020) Colocalized Particle Counting Platform for Zeptomole Level Multiplexed Quantification. Anal Chem 92:3697–3706.

3. Li X, Wei L, Pan L, Yi Z, Wang X, Ye Z, Xiao L, Li H-W, Wang J (2018) Homogeneous Immunosorbent Assay Based on Single-Particle Enumeration Using Upconversion Nanoparticles for the Sensitive Detection of Cancer Biomarkers. Anal Chem 90:4807–4814.

4. Pei X, Yin H, Lai T, Zhang J, Liu F, Xu X, Li N (2018) Multiplexed Detection of Attomoles of Nucleic Acids Using Fluorescent Nanoparticle Counting Platform. Anal Chem 90:1376–1383.

5. Ray P, Steckl AJ (2019) Label-Free Optical Detection of Multiple Biomarkers in Sweat, Plasma, Urine, and Saliva. ACS Sens 4:1346–1357.

6. Steckl AJ, Ray P (2018) Stress Biomarkers in Biological Fluids and Their Point-of-Use Detection. ACS Sens 3:2025–2044.

7. Tu E, Pearlmutter P, Tiangco M, Derose G, Begdache L, Koh A (2020) Comparison of Colorimetric Analyses to Determine Cortisol in Human Sweat. ACS Omega 5:8211–8218.

8. Dalirirad S, Han D, Steckl AJ (2020) Aptamer-Based Lateral Flow Biosensor for Rapid Detection of Salivary Cortisol. ACS Omega 5:32890–32898.

9. Calmo R, Chiadò A, Fiorilli S, Ricciardi C (2020) Advanced ELISA-like Biosensing Based on Ultralarge-Pore Silica Microbeads. ACS Appl Bio Mater 3:5787–5795.

10. Zhang Z, Chen Z, Wang S, Cheng F, Chen L (2015) Iodine-Mediated Etching of Gold Nanorods for Plasmonic ELISA Based on Colorimetric Detection of Alkaline Phosphatase. ACS Appl Mater Interfaces 7:27639–27645.

11. Gao Y, Zhou Y, Chandrawati R (2020) Metal and Metal Oxide Nanoparticles to Enhance the Performance of Enzyme-Linked Immunosorbent Assay (ELISA). ACS Appl Nano Mater 3:1–21.

12. Zhao C, Pan B, Wang M, Si Y, Taha AY, Liu G, Pan T, Sun G (2022) Improving the Sensitivity of Nanofibrous Membrane-Based ELISA for On-Site Antibiotics Detection. ACS Sens 7:1458–1466.

13. Sun J, Zhao J, Wang L, Li H, Yang F, Yang X (2018) Inner Filter Effect-Based Sensor for Horseradish Peroxidase and Its Application to Fluorescence Immunoassay. ACS Sens 3:183–190.

14. Natarajan S, Su F, Jayaraj J, Shah MII, Huang Y (2019) A paper microfluidics-based fluorescent lateral flow immunoassay for point-of-care diagnostics of non-communicable diseases. Analyst 144:6291–6303.

15. Nayan V, Sinha ES, Onteru SK, Singh D (2020) A proof-of-concept of lateral flow based luteinizing hormone detection in urine for ovulation prediction in buffaloes. Anal Methods 12:3411–3424.

16. Hossain SMZ, Luckham RE, McFadden MJ, Brennan JD (2009) Reagentless Bidirectional Lateral Flow Bioactive Paper Sensors for Detection of Pesticides in Beverage and Food Samples. Anal Chem 81:9055–9064.

17. Xu Y, Liu Y, Wu Y, Xia X, Liao Y, Li Q (2014) Fluorescent Probe-Based Lateral Flow Assay for Multiplex Nucleic Acid Detection. Anal Chem 86:5611–5614.

18. Alam N, Tong L, He Z, Tang R, Ahsan L, Ni Y (2023) Mechanically Compressed Barriers Improve Paper-Based Lateral Flow Assay Sensitivity for COVID-19 Nucleic Acid Detection. Ind Eng Chem Res 62:18800–18809.

19. P. K. S, Bathula C, K. N. C, Das M (2020) Usage of Graphene Oxide in Fluorescence Quenching-Linked Immunosorbent Assay for the Detection of Cry2Ab Protein Present in Transgenic Plants. J Agric Food Chem 68:3656–3662.

20. Tian Y, Xin C, Liu S, Liu Y, Liu S (2018) Affinity Binding-Induced Hg^{2+} Release and Quantum Dot Doping for General, Label-Free, and Homogenous Fluorescence Protein Assay. ACS Sens 3:1401–1408.

21. Lin B, Sun Q, Liu K, Lu D, Fu Y, Xu Z, Zhang W (2014) Label-Free Colorimetric Protein Assay and Logic Gates Design Based on the Self-assembly of Hemin-Graphene Hybrid Nanosheet. Langmuir 30:2144–2151.

22. Wan G-Z, Chen J (2024) Cerium-Based Metal–Organic Framework Nanocrystals for Colorimetric Screening of α-Glucosidase Inhibitors. ACS Appl Nano Mater 7:13636-13648.

23. Zhang Q, Fu Y, Xiao K, Du C, Zhang X, Chen J (2021) Sensitive Dual-Mode Biosensors for CYFRA21-1 Assay Based on the Dual-Signaling Electrochemical Ratiometric Strategy and “On–Off–On” PEC Method. Anal Chem 93:6801–6807.

24. Samper IC, McMahon CJ, Schenkel MS, Clark KM, Khamcharoen W, Anderson LBR, Terry JS, Gallichotte EN, Ebel GD, Geiss BJ, Dandy DS, Henry CS (2022) Electrochemical Immunoassay for the Detection of SARS-CoV-2 Nucleocapsid Protein in Nasopharyngeal Samples. Anal Chem 94:4712–4719.

25. Beeg M, Nobili A, Orsini B, Rogai F, Gilardi D, Fiorino G, Danese S, Salmona M, Garattini S, Gobbi M (2019) A Surface Plasmon Resonance-based assay to measure serum concentrations of therapeutic antibodies and anti-drug antibodies. Sci Rep 9:2064-2073.

26. Basso CR, Malossi CD, Haisi A, Pedrosa V de A, Barbosa AN, Grotto RT, Junior JPA (2021) Fast and reliable detection of SARS-CoV-2 antibodies based on surface plasmon resonance. Anal Methods 13:3297–3306.

27. Fujinami Tanimoto IM, Cressiot B, Jarroux N, Roman J, Patriarche G, Le Pioufle B, Pelta J, Bacri L (2021) Selective target protein detection using a decorated nanopore into a microfluidic device. Biosens Bioelectron 183:113195-113203.

28. Zhang Y, Chen X, Wang C, Roozbahani GM, Chang H-C, Guan X (2020) Chemically functionalized conical PET nanopore for protein detection at the single-molecule level. Biosens Bioelectron 165:112289-112297.

29. Nam J-M, Stoeva SI, Mirkin CA (2004) Bio-Bar-Code-Based DNA Detection with PCR-like Sensitivity. J Am Chem Soc 126:5932–5933.

30. Hill HD, Vega RA, Mirkin CA (2007) Nonenzymatic Detection of Bacterial Genomic DNA Using the Bio Bar Code Assay. Anal Chem 79:9218–9223.

31. Tao X, Chang X, Wan X, Guo Y, Zhang Y, Liao Z, Song Y, Song E (2020) Impact of Protein Corona on Noncovalent Molecule–Gold Nanoparticle-Based Sensing. Anal Chem 92:14990–14998.

32. Lin J-H, Chang C-W, Wu Z-H, Tseng W-L (2010) Colorimetric Assay for S-Adenosylhomocysteine Hydrolase Activity and Inhibition Using Fluorosurfactant-Capped Gold Nanoparticles. Anal Chem 82:8775–8779.

33. Alsager OA, Kumar S, Zhu B, Travas-Sejdic J, McNatty KP, Hodgkiss JM (2015) Ultrasensitive Colorimetric Detection of 17β-Estradiol: The Effect of Shortening DNA Aptamer Sequences. Anal Chem 87:4201–4209.

34. Zeng T, Fang J, Jiang Y, Xing C, Lu C, Yang H (2022) Spherical Nucleic Acid Probe Based on 2'-Fluorinated DNA Functionalization for High-Fidelity Intracellular Sensing. Anal Chem 94:18009–18016.

35. Wu B, Chen N, Wang Q, Yang X, Wang K, Li W, Li Q, Liu W, Fang H (2016) A simple label-free aptamer-based method for C-reactive protein detection. Anal Methods 8:4177–4180.

36. Xing Y, Gao Q, Zhang Y, Ma L, Loh KY, Peng M, Chen C, Cui Y (2017) The improved sensitive detection of C-reactive protein based on the chemiluminescence immunoassay by employing monodispersed PAA-Au/Fe3O4 nanoparticles and zwitterionic glycerophosphoryl choline. J Mater Chem B 5:3919–3926.

37. Yuan Z, Han M, Li D, Hao R, Guo X, Sang S, Zhang H, Ma X, Jin H, Xing Z, Zhao C (2023) A cost-effective smartphone-based device for rapid C-reaction protein (CRP) detection using magnetoelastic immunosensor. Lab Chip 23:2048–2056.

38. Rong Z, Xiao R, Xing S, Xiong G, Yu Z, Wang L, Jia X, Wang K, Cong Y, Wang S (2018) SERS-based lateral flow assay for quantitative detection of C-reactive protein as an early bio-indicator of a radiation-induced inflammatory response in nonhuman primates. Analyst 143:2115–2121.

39. Jang Y, Kim H, Yang SY, Jung J, Oh J (2020) Bioactive multiple-bent MWCNTs for sensitive and reliable electrochemical detection of picomolar-level C-reactive proteins. Nanoscale 12:9980–9990.

40. Zhou Y, Ding Y, Huang Y, Cai L, Xu J, Ma X (2020) Synthesis and Structural Optimization of Iridium(III) Solvent Complex for Electrochemiluminescence Labeling of Histidine-Rich Protein and Immunoassay Applications for CRP Detection. ACS Omega 5:3638–3645.

41. Ma J, Li S, Huang X, Jiang J, Xu T, Liu T (2024) All Optic-Fiber Waveguide-Coupled SPR Sensor for CRP Sensing Based on Dielectric Layer and Poly-Dopamine. Photonic Sens 15:250224-2502236.

42. Cierpiak K, Wityk P, Kosowska M, Sokołowski P, Talaśka T, Gierowski J, Markuszewski MJ, Szczerska M (2024) C-reactive protein (CRP) evaluation in human urine using optical sensor supported by machine learning. Sci Rep 14:18854-18866.

43. Grewal R, Ortega GA, Geng F, Srinivasan S, Rajabzadeh AR (2024) Label-free electrochemical detection of glycated hemoglobin (HbA1c) and C-reactive protein (CRP) to predict the maturation of coronary heart disease due to diabetes. Bioelectrochemistry 159:108743-108753.

44. Malekmohamadi M, Mirzaei S, Rezayan AH, Abbasi V, Abouei Mehrizi A (2024) µPAD-based colorimetric nanogold aptasensor for CRP and IL-6 detection as sepsis biomarkers. Microchem J 197:109744-109754.

45. Wilson CS, Vashi B, Genzor P, Gregory MK, Yau J, Wolfe L, Lochhead MJ, Papst P, Pettrone K, Blair PW, Krishnan S, Chenoweth JG, Clark DV (2023) Point-of-care biomarker assay for rapid multiplexed detection of CRP and IP-10. SLAS Technol 28:442–448.

46. Hosseinniay S, Rezayan AH, Ghasemi F, Malekmohamadi M, Taheri RA, Hosseini M, Alvandi H (2023) Fabrication and evaluation of optical nanobiosensor based on localized surface plasmon resonance (LSPR) of gold nanorod for detection of CRP. Anal Chim Acta 1237:340580-340588.

47. Szot-Karpińska K, Kudła P, Orzeł U, Narajczyk M, Jönsson-Niedziółka M, Pałys B, Filipek S, Ebner A, Niedziółka-Jönsson J (2023) Investigation of Peptides for Molecular Recognition of C-Reactive Protein–Theoretical and Experimental Studies. Anal Chem 95:14475–14483.

48. Zhang Y, Rojas OJ (2017) Immunosensors for C-Reactive Protein Based on Ultrathin Films of Carboxylated Cellulose Nanofibrils. Biomacromolecules 18:526–534.

49. Fan L, Yan W, Chen Q, Tan F, Tang Y, Han H, Yu R, Xie N, Gao S, Chen W, Chen Z, Zhang P (2024) One-Component Dual-Readout Aggregation-Induced Emission Nanobeads for Qualitative and Quantitative Detection of C-Reactive Protein at the Point of Care. Anal Chem 96:401–408.

50. Yan H, Hu X, Shao H, Li J, Deng J, Liu L (2023) Low-Cost Full-Range Detection of C-Reactive Protein in Clinical Samples by Aptamer Hairpin Probes and Coprecipitation of Silver Ions and Gold Nanoparticles. Anal Chem 95:11918–11925.

51. Boonkaew S, Chaiyo S, Jampasa S, Rengpipat S, Siangproh W, Chailapakul O (2019) An origami paper-based electrochemical immunoassay for the C-reactive protein using a screen-printed carbon electrode modified with graphene and gold nanoparticles. Microchim Acta 186:153-154.

52. Zhang L, Li H-Y, Li W, Shen Z-Y, Wang Y-D, Ji S-R, Wu Y (2018) An ELISA Assay for Quantifying Monomeric C-Reactive Protein in Plasma. Front Immunol 9.

53. Walter J-G, Eilers A, Alwis LSM, Roth BW, Bremer K (2020) SPR Biosensor Based on Polymer Multi-Mode Optical Waveguide and Nanoparticle Signal Enhancement. Sensors 20:2889-2900.

54. Vashist SK, Marion Schneider E, Zengerle R, von Stetten F, Luong JHT (2015) Graphene-based rapid and highly-sensitive immunoassay for C-reactive protein using a smartphone-based colorimetric reader. Biosens Bioelectron 66:169–176.

55. Petruzzi L, Maier T, Ertl P, Hainberger R (2022) Quantitative detection of C-reactive protein in human saliva using an electrochemical lateral flow device. Biosens Bioelectron 10:100136-100146.

56. Zhang Y, Chen X, Wang C, Chang H-C, Guan X (2022) Nanoparticle-assisted detection of nucleic acids in a polymeric nanopore with a large pore size. Biosens Bioelectron 196:113697-113705.

57. Xu Q, Lou X, Wang L, Ding X, Yu H, Xiao Y (2016) Rapid, Surfactant-Free, and Quantitative Functionalization of Gold Nanoparticles with Thiolated DNA under Physiological pH and Its Application in Molecular Beacon-Based Biosensor. ACS Appl Mater Interfaces 8:27298–27304.

58. Khashayar P, Amoabediny G, Larijani B, Hosseini M, Vanfleteren J (2017) Fabrication and Verification of Conjugated AuNP-Antibody Nanoprobe for Sensitivity Improvement in Electrochemical Biosensors. Sci Rep 7:16070-16078.

59. Zhang X, Gouriye T, Göeken K, Servos MR, Gill R, Liu J (2013) Toward Fast and Quantitative Modification of Large Gold Nanoparticles by Thiolated DNA: Scaling of Nanoscale Forces, Kinetics, and the Need for Thiol Reduction. J Phys Chem C 117:15677–15684.

60. Li J, Zhu B, Yao X, Zhang Y, Zhu Z, Tu S, Jia S, Liu R, Kang H, Yang CJ (2014) Synergetic Approach for Simple and Rapid Conjugation of Gold Nanoparticles with Oligonucleotides. ACS Appl Mater Interfaces 6:16800–16807.

61. Hurst SJ, Lytton-Jean AKR, Mirkin CA (2006) Maximizing DNA Loading on a Range of Gold Nanoparticle Sizes. Anal Chem 78:8313–8318.

62. Wang S, Luo J, He Y, Chai Y, Yuan R, Yang X (2018) Combining Porous Magnetic Ni@C Nanospheres and $CaCO_3$ Microcapsule as Surface-Enhanced Raman Spectroscopy Sensing Platform for Hypersensitive C-Reactive Protein Detection. ACS Appl Mater Interfaces 10:33707–33712.

63. Hong D, Kim K, Jo E-J, Kim M-G (2021) Electrochemiluminescence-Incorporated Lateral Flow Immunosensors Using $Ru(bpy)_3^{2+}$-Labeled Gold Nanoparticles for the Full-Range Detection of Physiological C-Reactive Protein Levels. Anal Chem 93:7925–7932.

64. Lee JS, Joung H-A, Kim M-G, Park CB (2012) Graphene-Based Chemiluminescence Resonance Energy Transfer for Homogeneous Immunoassay. ACS Nano 6:2978–2983.

65. Jampasa S, Siangproh W, Laocharoensuk R, Vilaivan T, Chailapakul O (2018) Electrochemical detection of c-reactive protein based on anthraquinone-labeled antibody using a screen-printed graphene electrode. Talanta 183:311–319.

66. Whitehouse WL, Lo LHY, Kinghorn AB, Shiu SCC, Tanner JA (2024) Structure-Switching Electrochemical Aptasensor for Rapid, Reagentless, and Single-Step Nanomolar Detection of C-Reactive Protein. ACS Appl Bio Mater 7:3721-3730.

67. Liu G, Zhang K, Nadort A, Hutchinson MR, Goldys EM (2017) Sensitive Cytokine Assay Based on Optical Fiber Allowing Localized and Spatially Resolved Detection of Interleukin-6. ACS Sens 2:218–226.

68. Zhao M, Yang Y, Li N, Lv Y, Jin Q, Wang L, Shi Y, Zhang Y, Shen H, Li LS, Wu R (2024) Development of a Dual Fluorescence Signal-Enhancement Immunosensor Based on Substrate Modification for Simultaneous Detection of Interleukin-6 and Procalcitonin. Langmuir 40:4447–4459.

69. Deng F, Arman A, Goldys EM, Hutchinson MR, Liu G (2020) A Method for in Vivo Quantification Of Cytokine IL-1β In The Rat Intrathecal Space. ACS Appl Bio Mater 3:539–546.

70. Calzaferri F, Narros-Fernández P, de Pascual R, de Diego AMG, Nicke A, Egea J, García AG, de los Ríos C (2021) Synthesis and Pharmacological Evaluation of Novel Non-nucleotide Purine Derivatives as P2X7 Antagonists for the Treatment of Neuroinflammation. J Med Chem 64:2272–2290.

71. Yang L, Fan D, Zhang Y, Ding C, Wu D, Wei Q, Ju H (2019) Ferritin-Based Electrochemiluminescence Nanosurface Energy Transfer System for Procalcitonin Detection Using HWRGWVC Heptapeptide for Site-Oriented Antibody Immobilization. Anal Chem 91:7145–7152.

72. Li Y, Liu W, Jin G, Niu Y, Chen Y, Xie M (2018) Label-Free Sandwich Imaging Ellipsometry Immunosensor for Serological Detection of Procalcitonin. Anal Chem 90:8002–8010.

Highlights

- We developed an enzyme-free fluorescent assay for rapid detection of CRP.
- The sensor was sensitive and selective with a limit of detection reaching ~27 fM.
- The method's high sensitivity was achieved via functionalized gold nanoparticles.
- Simulated serum samples were successfully analyzed.